

Journal of Materials Chemistry A

Accepted Manuscript



This is an *Accepted Manuscript*, which has been through the Royal Society of Chemistry peer review process and has been accepted for publication.

Accepted Manuscripts are published online shortly after acceptance, before technical editing, formatting and proof reading. Using this free service, authors can make their results available to the community, in citable form, before we publish the edited article. We will replace this *Accepted Manuscript* with the edited and formatted *Advance Article* as soon as it is available.

You can find more information about *Accepted Manuscripts* in the [Information for Authors](#).

Please note that technical editing may introduce minor changes to the text and/or graphics, which may alter content. The journal's standard [Terms & Conditions](#) and the [Ethical guidelines](#) still apply. In no event shall the Royal Society of Chemistry be held responsible for any errors or omissions in this *Accepted Manuscript* or any consequences arising from the use of any information it contains.

High-rate aqueous symmetric pseudocapacitor based on highly graphitized onion-like carbon/birnessite-type manganese oxide nanohybrids

Katlego Makgopa,¹ Paul M. Ejikeme,¹ Charl J. Jafta,² Kumar Raju,²
Marco Zeiger,^{3,4} Volker Presser,^{3,4*} and Kenneth I. Ozoemena^{1,2*}

¹ *Department of Chemistry, University of Pretoria, Pretoria 0002, South Africa*

² *Energy Materials, Materials Science and Manufacturing, Council for Scientific & Industrial Research (CSIR), Pretoria 0001, South Africa*

³ *INM - Leibniz Institute for New Materials, 66123 Saarbrücken, Germany*

⁴ *Saarland University, 66123 Saarbrücken, Germany*

*Authors to whom correspondence should be addressed:

(K.I. Ozoemena): Tel.: +27128413664; Fax: +27128412135; E-mail: kozoemena@csir.co.za;

(V. Presser): Tel.: +496819300177; Fax: +496819300223; E-mail: volker.presser@inm-gmbh.de

Abstract

We present a study on the pseudocapacitive properties of birnessite-type MnO_2 grafted on highly graphitized onion-like carbon (OLC/ MnO_2). In a three-electrode setup, we evaluated two different substrates, namely a platinum disc and nickel foam. The OLC/ MnO_2 nanohybrid gave large specific capacitance (C_{sp}) of 295 and 323 F g^{-1} (at 1 A g^{-1}) for the Pt disc and Ni foam, respectively. In addition, the Ni foam substrate exhibited much higher rate capability (power density) than the Pt disc. A symmetrical two-electrode device, fabricated with the Ni foam, showed a large C_{sp} of 254 F g^{-1} , specific energy density of 5.6 Wh kg^{-1} , and a high power density of 74.8 kW kg^{-1} . These values are the highest for onion-based electrodes so far. The device showed excellent capacity retention when subjected to voltage-holding (floating) experiments for 50 h. In addition, the device showed low equivalent distributed resistance ($\text{EDR} \approx 3 \Omega \text{ cm}^2$) with very short time constant ($\tau = 40 \text{ ms}$). This high rate handling ability of the OLC/ MnO_2 nanohybrid, compared to literature reports, promises new opportunities for the development of aqueous-based pseudocapacitors.

Keywords: Energy storage; pseudocapacitor; onion-like carbon; birnessite-type manganese dioxide; voltammetry; impedance spectroscopy

Introduction

Supercapacitors are advanced systems for electrochemical energy storage.^{1,2} Two different types of supercapacitors can be differentiated: (a) electrical double-layer capacitors (EDLC) that only rely on charge storage via ion electrosorption in the electrical double-layer, and (b) pseudocapacitors that utilize fast (surface) redox reactions.³⁻⁶ Over the last years, supercapacitors have attracted tremendous attention due to their excellent properties such as high power density, long cycle ability, high efficiency, and relying on abundantly available carbon materials.^{7,8} Considering energy and power performance, supercapacitors play a key role as intermediate between batteries and electrolytic capacitors⁹ and find widespread applications for fast charge/discharge and uninterrupted power supply applications as well as in combination with batteries in hybrid systems.¹⁰ There have been extensive studies of varieties of carbon materials for supercapacitor electrodes because of their large specific surface area (SSA), high conductivity, facile availability, and chemical stability.^{5,11} Some of the best performing carbon materials include activated carbon,¹² carbon nanotubes (CNTs),¹³ graphene,^{14,15} carbon nanofibers (CNFs),^{16,17} and carbon aerogels.¹⁸

Among carbon nanomaterials, non-porous carbon onions, also known as onion-like carbon (OLC), have attracted major research interests as electrode material for energy storage, for example, advanced anode electrodes for lithium ion batteries,^{19,20} pseudocapacitors,^{21,22} and ultrahigh-power electric double-layer capacitors.²³⁻²⁵ The major attractions stem from the ability to prepare them on a large-scale by thermal annealing of nanodiamonds and the superior power handling ability.²⁶ OLCs are described as multi-shell fullerenes²⁷ that, unlike fullerenes, exhibit a high electrical conductivity commonly in the range of 2-4 S cm⁻¹.²⁵ However, the limited surface area of OLCs (200-600 m² g⁻¹ range) have also resulted in limited double-layer capacitance (usually between 25 and 50 F g⁻¹, equivalent up to 2 Wh kg⁻¹ at 1 V).^{25,26}

OLCs derived from thermal treatment of nanodiamonds (ND)²⁸ are highly graphitic spherical particles (5-10 nm) that consist of concentric carbon shells.²⁹ Alternative synthesis methods may yield also larger OLCs with diameters of more than 10 nm^{19,30} and include condensation of carbon vapor,³¹ or electron beam irradiation.³² However, thermal annealing of ND³³ at temperatures between 1000 and 2000 °C is currently the preferred technique to synthesize OLC since large amounts of material can be obtained.³⁴ Also, a narrow size distribution of the ND precursor translates into a narrow size distribution of resulting onion-like carbons.²¹

Birnessite-type MnO₂ (in this paper referred to just “MnO₂”) exhibits a two-dimensional layered structure (see *Supporting Information, Fig. S1*) displaying edge-sharing MnO₆ octahedra in the sheets, metal cations (for example K⁺) and water molecules in the interlayer region. Hence, an appropriate chemical representation would be K_xMn₂O₄·yH₂O (with $x \leq 0.5$ and $y \leq 1.5$).³⁵ This metal oxide has become an attractive electrode material for an efficient and low-cost development of supercapacitor due to its natural abundance and environmental compatibility.^{36,37-41,42} However, because of its low electrical conductivity (10⁻⁶-10⁻⁵ S cm⁻¹) and poor power handling capability, electrochemical performance of MnO₂ electrodes is rather low, which significantly limits its potential applications as high-power supercapacitors.⁴³ The capacitive performance, redox activity, as well as utilization of MnO₂ can be enhanced by addition of conductive materials.⁴⁴⁻⁴⁶ However, the resulting performance strongly depends on the quality and properties of such carbon/metal oxide hybrid materials.

This work, for the first time, reports the electrochemistry of MnO₂ integrated with highly graphitized OLCs derived from NDs (herein abbreviated simply as OLC/MnO₂ nanohybrid) as high-power pseudocapacitor in a neutral aqueous medium (1 M Na₂SO₄). Previous works related to MnO₂ with “carbon onions” was carried out using low-graphitized

material obtained from either clarified butter (“Ghee”)³⁰ or phenolic-formaldehyde resins with much larger particle diameters (tens of nm).⁴² Whilst these initial reports encouraging, we show in this study that by using highly graphitized OLCs, the OLC/MnO₂ nanohybrids exhibit a very high power density ($\sim 75 \text{ kW kg}^{-1}$). In addition, our devices show excellent capacitance retention upon long-hour voltage-holding and very low equivalent distribution resistance ($\text{EDR} \approx 3 \Omega \text{ cm}^2$) with a response time of just a few milliseconds.

Experimental section

Precursor and synthesis of OLC and OLC/MnO₂

OLC was synthesized from nanodiamond (ND) powder with a purity of 98-99 % (NaBond Technologies) and thoroughly characterized as recently described.⁴⁷ Briefly, ND powder was placed in a closed-lid cylindrical graphite crucibles (30 mm in diameter and 20 mm in height) and thermally annealed in a water-cooled high temperature vacuum furnace with tungsten heaters (Model: 1100-3580-W1, Thermal Technology Inc.). The heating and cooling rate were both $15 \text{ }^\circ\text{C min}^{-1}$ and the chamber pressure ranged between 10 and 100 mPa. The final OLC was annealed at $1750 \text{ }^\circ\text{C}$ for 3 h. The OLC/MnO₂ nanohybrid material was prepared using the conventional hydrothermal reduction technique. Typically, 40 mg of OLC was dispersed by sonication in 30 mL of 0.02 M KMnO₄ (Merck), and the mixture ($\text{pH} = 7.05$) was refluxed at $130 \text{ }^\circ\text{C}$ in an oil bath for 24 h with continuous magnetic stirring. The resultant dispersion was then centrifuged and washed several times with deionized water, and finally dried at $60 \text{ }^\circ\text{C}$ overnight in a vacuum oven. All chemicals were of analytical grade and used as received. Deionized water was used throughout the synthesis process.

Structural characterization

Surface morphology characterization of the samples was obtained using a JSM-7500F (JEOL, Japan) scanning electron microscope (SEM) operated at 3.0 kV. Energy dispersive X-ray spectra (EDX) were measured with an EDX system (Oxford Instruments) at 5 different positions. The chemical composition was calculated using the AZtec energy analysis software (Oxford Instruments). Transmission electron microscopy (TEM) samples were prepared by dispersing powders in ethanol and placing the solution over a copper grid with a lacey carbon film. All measurements were carried out with a 2100F microscope (JEOL) operating at 200 kV. X-ray diffraction (XRD) patterns of the samples were collected using an X'Pert-Pro MPD diffractometer (PANalytical) with theta/theta geometry (step width: $0.0263^\circ \text{ s}^{-1}$), operating a copper tube at 40 kV and 40 mA. The instrumental resolution function was characterized with the NIST SRM 660a (LaB_6) standard. The patterns were recorded in the range of $5\text{-}148^\circ 2\theta$. Qualitative phase analysis of the samples was conducted using Bruker EVA using the PDF database.

Raman spectra were recorded with a Renishaw inVia Raman microscope using an Nb-YAG laser with an excitation wavelength of 532 nm and a grating with $1800 \text{ lines mm}^{-1}$ yielding a spectral resolution of *ca.* 1.2 cm^{-1} . The spot size on the sample was in the focal plane *ca.* $2 \mu\text{m}$ using an output power of 0.5 mW. Spectra were recorded for 30 s and accumulated 50 times to eliminate cosmic rays and to obtain a high signal-to-noise and signal-to-background ratio. Peak fitting was achieved by employing Lorentzian peaks assuming four components for the carbon spectrum between 1000 and 1800 cm^{-1} . Fourier infrared spectroscopy (FTIR) analyses were carried out using Perkin Elmer FT-IR spectrophotometer. OLC and OLC/ MnO_2 nanohybrids were analyzed as KBr pellets (10 scans).

X-ray photoelectron spectroscopy (XPS) experiments were carried out on a Kratos Axis Ultra-DLD system (Shimadzu) with monochromated Al $K\alpha$ radiation (1486.6 eV).

Binding energies were calibrated using the containment carbon (C 1s @ 284.6 eV). The spectra analysis was performed with the XPS Peak 4.1 program and a Shirley function was used to subtract the background. The metal oxide content in the nanohybrid was determined by thermogravimetric analysis (TGA) using an STA Jupiter 449 C (Netzsch) in Ar/O₂ atmosphere at a temperature scan rate of 10 K min⁻¹.

Nitrogen gas sorption measurements were made with a Quantachrome Autosorb iQ system. The samples were outgassed at 150 °C for 10 h under vacuum condition. Gas sorption was performed in liquid nitrogen (-196 °C) with relative pressure range from 10⁻⁷ to 0.95 in 68 steps. The specific surface area (SSA) was calculated with the ASQwin-software using Brunauer-Emmett-Teller (BET) equation⁴⁸ in the relative pressure range 0.01-0.2. We also calculated SSA and pore size distribution (PSD) via quenched-solid density functional theory (QSDFT)⁴⁹ with hybrid model for slit and cylindrical pores and pore size between 0.56 and 37.5 nm.

Electrochemical characterization

All electrochemical measurements were carried out using a Bio-Logic VMP 300 potentiostat/galvanostat using either a three-electrode (half-cell) or a two-electrode (full cell) configuration. For the three-electrode configurations a Pt disc and Nickel foam were used as substrates for the working electrodes. For the three-electrode configuration using Pt disc, a custom-built three-electrode cell (cf. Ref. [47]) was used. The working electrode was prepared by drop-casting 7.1 mg mL⁻¹ OLC colloidal dispersion (10 mass% polyvinylidenefluoride, PVDF in ethanol) or 9.0 mg mL⁻¹ OLC/MnO₂ nanohybrid colloidal dispersion (in anhydrous N-methyl-2-pyrrolidone, NMP) onto a Pt disc (diameter: 12 mm, thickness: 100 μm, purity 99.99 %, Carl Schaefer) and dried at 80 °C overnight in a vacuum oven at 20 mbar to remove the solvent. Polytetrafluoroethylene (PTFE) bound (5 % in total electrode mass) activated carbon (YP50F, Kuraray Chemical) served as counter electrode and

was largely oversized in charge capacity as compared to the working electrode. A platinum wire (diameter 1 mm, purity 99.99 %, Carl Schaefer) served as a pseudo-reference electrode. For the nickel foam based three-electrode configuration, the nickel foam (Celmet: thickness = 1.6 mm, surface area = $7500 \text{ m}^2 \text{ m}^{-3}$, cell size = 0.5 mm, 48-52 cells per inch) was cleaned prior to use, in a 1 M HCl solution, washed with a copious amount of de-ionized water to a neutral pH, and dried under vacuum. It was pasted with a mixture of OLC/MnO₂ nanohybrid, carbon black (CB, Degussa), and polyvinylidene fluoride (PVDF) (mass% of 80:15:5 respectively, homogeneously mixed with a few drops of anhydrous N-methyl-2-pyrrolidone using paste pestle and mortar). The CB and PVDF served as conductive additive and binder, respectively. The electrode was then dried at 80 °C overnight in a vacuum oven, and pressed to a thickness of 250 μm. The electrode was cut to a 1 cm x 1 cm, while the mass loading was typically 1 mg cm^{-2} for the Pt disc and nickel foam. An over-sized glassy carbon plate ($1.6 \times 1.6 \text{ cm}^2$) was used as the counter electrode and Ag/AgCl (3 M KCl) as the reference electrode. The two-electrode configuration was fabricated using the nickel foam as substrate. Both the positive and negative electrodes used nickel foam coated with the OLC/MnO₂ nanohybrid, obtained as described for the three-electrode above. The resulting slurry was coated onto the nickel foam substrate ($\sim 3 \text{ cm}^2$) with a spatula using an average mass loading of 1 mg cm^{-2} . Symmetric cells were also prepared using nickel foam loaded with only OLC. In all experiments, 1 M Na₂SO₄ was used as electrolyte and a porous glass fiber (Whatman Grade GF/D Glass Microfiber Filters, Sigma-Aldrich) served as the separator. For the three-electrode configuration, cyclic voltammetry was performed at various scan rates (2-100 mV s^{-1}). Voltage-holding (floating) experiments were performed for 10 h at 0.8 V, then galvanostatically charged-discharged between 0.0 and 0.8 V at 1 A g^{-1} , repeating the process for five times (i.e., total of 50 h). Electrochemical impedance spectroscopy (EIS) data were obtained between 100 kHz and 10 mHz with a perturbation amplitude (rms value) of the AC

signal of 2 mV. Every EIS experiment was performed after allowing the cell to equilibrate for 5 min at the chosen fixed potential.

The specific capacitance (C_{sp}) for the half-cells, obtained from CV and galvanostatic discharge curves were evaluated using the established equation (1) and (2), respectively.

$$C_{sp} \left(\frac{F}{g} \right) = \frac{\int idt}{\Delta V \cdot m} \quad (1)$$

$$C_{sp} \left(\frac{F}{g} \right) = \frac{i\Delta t}{\Delta V \cdot m} \quad (2)$$

where: i (A) is the current, ΔV (V)/ Δt (s) the slope of the discharge curve, and m (g) the mass of active electrode, V (V) is the voltage obtained during charge. Note that the iR drop ranged from 3.2 to 1.1 Ω at the current densities of 0.1-10 A g^{-1} .

The specific capacitance (C_{sp}), maximum specific power density (P_{max}) and specific energy density (E_{sp}) for the full cells (symmetric devices) were evaluated from the slope of the charge-discharge curves using equations (3-6).¹

$$C(F) = \frac{i}{\Delta V/\Delta t} \quad (3)$$

$$C_{sp} \left(\frac{F}{g} \right) = \frac{4 \cdot C}{m} \quad (4)$$

$$P_{max} \left(\frac{10^3 \text{ W}}{\text{kg}} \right) = \frac{V^2}{4mR_s} \quad (5)$$

$$E \left(\frac{1}{3.6} \frac{\text{Wh}}{\text{kg}} \right) = \frac{CV^2}{2m} \quad (6)$$

where i (A) is the applied current, ΔV (V)/ Δt (s) the slope of the discharge curve and m (g) the total mass of both electrodes, C (F) the calculated capacitance, V (V) is the maximum voltage obtained during charge, and R_s is the equivalent series resistance (ESR).

Results and Discussion

SEM, TEM, and gas sorption analysis

The surface morphologies of OLC and OLC/MnO₂ nanohybrid studied using FESEM are shown in **Fig. 1a&c** and using TEM in **Fig. 1b&d**. The primary particle size of carbon onions is in the range of a few nanometers as seen from the TEM images in agreement with our previous findings.⁴⁷ This primary particle size is maintained for the OLC/MnO₂ nanohybrid. Compared with OLC, OLC/MnO₂ hybrid nanoparticles exhibited an obviously different morphology. The SAED pattern in the inset (**Fig. 1d**) shows lattice fringes for crystalline MnO₂ and circular lattice shells for OLC [30]. Rather than a monolayer or multilayer coating of each carbon onion, an effective OLC/MnO₂ nanohybrid was obtained with nanodomains of highly mixed graphitic carbon and metal oxide. The amount of metal oxide was determined by TGA to represent 47 mass% of the OLC/MnO₂ nanohybrid material (see *Supporting Information*, **Fig. S2**). Also, the TGA data shows the excellent thermal stability of OLC with an onset of oxidation at around 630 °C as a result of the highly graphitic character of carbon onions synthesized at 1750 °C.

Fig. 2 shows nitrogen gas sorption data for OLC and OLC/MnO₂ nanohybrid. As we see, OLC/MnO₂ exhibits a DFT SSA of 122 m² g⁻¹ with a distribution of micropores (<2 nm) and mesopores (between 2 and 50 nm). This represents a severe loss in specific surface area compared to OLC with a DFT SSA of 391 m² g⁻¹ and is mostly related with the higher molecular mass and higher density of MnO₂ in addition to pore blocking.⁵⁰ Yet, **Fig. 2a** shows that the overall pore size distribution is preserved after the addition of MnO₂ at a lower total pore volume.

XRD, Raman, FTIR, EDX, and XPS studies

Fig. 3 illustrates the Raman spectra, X-ray diffraction pattern, and FTIR spectra of OLC and the corresponding OLC/MnO₂ nanohybrid material. The presence of MnO₂ is confirmed by a strong Raman signal at around 565 cm⁻¹,⁵¹ (**Fig. 3a**). The presence of the OLC in the hybrid from the XRD analysis is confirmed by Raman peaks associated with the carbon D-mode (1350 cm⁻¹) and G-mode (1590 cm⁻¹) of OLC/MnO₂. Peak analysis (inset in **Fig. 3a**) shows that the hydrothermal synthesis only insignificantly changes the OLC structure: both D- and G-mode remain almost unchanged. In particular, the I_D/I_G ratios before and after MnO₂ deposition are almost identical with values of 1.20 and 1.25, respectively. The FWHM for both the D-mode and the G-mode were measured to 73.1 cm⁻¹ and 69.8 cm⁻¹ before the deposition and to 78.5 cm⁻¹ and 65.4 cm⁻¹ after the MnO₂ deposition. The only minor change related to the carbon signal is identified at around 1100 to 1200 cm⁻¹ which may indicate the formation of a small amount of functionalized carbon.⁵² FTIR was used to study further the electrode materials as shown by **Fig. 3c**. The well pronounce peak at 550 cm⁻¹ is due to Mn-O-Mn asymmetric stretching vibration. The broad peak at 3450 cm⁻¹ is assigned to hydroxyl groups which suggests that there are water molecules in the interlayers (see also structure given in the *Supporting Information*, **Fig. S1**).⁵³

From the XRD patterns of the OLC/MnO₂ nanohybrid (**Fig. 3b**), the peak at 2θ around 26° is associated with the (002) plane of graphitic carbon and it can be observed also in OLC/MnO₂ diffractograms indicating the presence of carbon in the nanohybrid. The other peaks can be indexed as birnessite-type MnO₂ (PDF 42-1317). All diffraction peaks of the metal oxide are broadened which indicates the nanocrystalline nature of the MnO₂ with an average coherence length (domain size) in the range of 5-10 nm. The calculated carbon *d*-spacing for the (002) plane is 0.352 nm and remains at that value with or without the

presence of MnO₂. This represents a small increase in lattice spacing compared to an ideal graphite crystal (i.e., 0.344 nm) as well-known for the carbon onion structure.⁵²

Chemical analysis confirms the presence of birnessite, meaning, not of pure MnO₂ but of a material following the average formula K_xMn₂O₄·yH₂O. Semi-quantitative analysis of OLC EDX spectra (**Fig. 4a** and **Table 1**) show less than 0.2 mass% of impurities alongside *ca.* 9 mass% of surface oxygen. The metal oxide shows an average molar Mn:K ratio of 4.6:1 which is somewhat larger than the maximum stoichiometric value of 4:1. The small difference might indicate the presence of minor amounts of residual KMnO₄. Yet, we note that the previously reported non-carbon content of around 47 mass% is in agreement with our EDX data (54.3 mass%). Only minor impurities of Si and Na can be detected which stem from impurities in the KMnO₄. XPS analysis of OLC/MnO₂ (**Fig. 4b**) shows the binding energy peaks of Mn and C. The Mn 2p region consisted of a spin-orbit doublet with Mn 2p_{1/2} and Mn 2p_{3/2} having binding energies of 654.2 eV and 642.3 eV, respectively.⁵⁴ The energy separation between Mn 2p_{1/2} and Mn 2p_{3/2}, of 11.9 eV is an indication of Mn in a +4 oxidation state.^{55–57} From the XPS survey scan, we also see the presence of significant amounts of K in addition to Mn, C, and O.

Table 1: Chemical composition of OLC and OLC/MnO₂ nanohybrid measured with EDX in mass% and atom%.

(mass%)	C	O	Na	Al	Si	K	Mn
OLC	90.8±1.7	9.1±1.7	-	0.2±0.1	-	-	-
OLC/MnO ₂	45.7±1.4	20.3±1.9	0.2±0.1	0.3±0.1	0.2±0.1	4.5±1.2	28.9±2.6

(atom%)	C	O	Na	Al	Si	K	Mn
OLC	93.0±1.3	7.0±1.3	-	0.1±0.1	-	-	-
OLC/MnO ₂	66.3±1.5	22.1±1.7	0.1±0.1	0.2±0.1	0.1±0.1	2.0±0.6	9.2±1.0

Comparative performance of half-cells at Pt disc and Ni foam

Fig. 5-6 compares the electrochemical performance of the three-electrode configurations using either a platinum disc (**Fig. 5**) or nickel foam (**Fig. 6**) as current collectors. The CV curves for OLC (**Fig. 5a**) are characteristic for double-layer capacitive materials, while the CV for OLC/MnO₂ nanohybrid shows redox-peaks indicative of faradic reactions (**Fig. 6a**). The same conclusions can be drawn from the galvanostatic charge / discharge profiles (**Fig. 5b-c** vs. **Fig. 6b-c**).^{58,59} We also see a high power handling ability of the materials with a comparatively small drop in specific capacitance of OLC/MnO₂ (335-180 F g⁻¹) as a function of the current density (0.3-32 A g⁻¹ range), **Fig. 6d**.

The key findings from **Fig. 5-6** may be summarized as follows: (i) The specific capacitance of the OLC/MnO₂ is more than a magnitude higher than that of the OLC for both current collectors (i.e., Ni foam and Pt disc); (ii) both types of current collectors gave essentially similar specific capacitance at different current densities (e.g., 250 F g⁻¹ at 5 A g⁻¹); and (iii) the stable voltage window for the Pt disc is narrower (0-0.5 V) than that of the nickel foam (0-1.0 V). The Nickel foam alone only insignificantly contributes to the charge storage mechanism (see *Supporting Information*, **Fig. S3**). We also note that carbon onions alone, that is without the presence of MnO₂, only exhibits a low specific capacitance of 12 F g⁻¹.

As summarized in **Table 2**, the maximum C_{sp} values for our 3-electrode tests (335-408 F g⁻¹ between 0.1 and 0.3 A g⁻¹) are much higher than those recorded in the literature. The impressive value (603 F g⁻¹ at 10 A g⁻¹) for electrodeposited MnO₂-nanopillars reported by Yu et al.⁷³ for their flexible nanostructured electrode obtained by combined sputter-coating and electrodeposition (PAN/Au-Pd/MnO₂, i.e., comprised a cocktail of polyacrylonitrile polymer and very expensive precious metals of palladium and gold) may, amongst other factors, be related to the thin film nature of their system and the mass of active

materials used in their calculations. Our values are somewhat comparable to those of the recent work by Ruoff et al.³⁹ involving the elaborate preparation of mesoporous nanotubes assembled from interwoven ultrathin birnessite-type MnO₂ nanosheets. Note that our result is much higher than that of the “OLC”/MnO₂ (~190 F g⁻¹ at 0.2 A g⁻¹) reported by Wang et al.,⁴² and the disparity can be related to the high graphitization of our OLC.

Table 2: Comparison of specific capacitance of various MnO₂-based three-electrode systems.

Samples	Electrolyte	C_{sp} (F g ⁻¹)	i (A g ⁻¹)	Reference
Birnessite-type MnO ₂	1 M Na ₂ SO ₄	335-408	0.1-0.3	This work
Birnessite-like hollow MnO ₂	1 M Na ₂ SO ₄	169	0.25	[37]
Birnessite-type MnO ₂ nanosphere	1 M Na ₂ SO ₄	210	1	[38]
Birnessite-type MnO ₂ nanotube	1 M Na ₂ SO ₄	365	0.25	[39]
Birnessite-type MnO ₂	1 M Na ₂ SO ₄	210	1	[40]
Birnessite-type MnO ₂ nanosheet	1 M Na ₂ SO ₄	269	0.3	[41]
Birnessite-type MnO ₂	1 M Na ₂ SO ₄	~190	0.2	[42]
Coral-like MnO ₂	1 M Na ₂ SO ₄	221	0.5	[63]
α -MnO ₂ ultralong nanowire	0.5 M Na ₂ SO ₄	345	1	[64]
α -MnO ₂ spherical-like particle	1 M Na ₂ SO ₄	259	0.1	[65]
α -MnO ₂ sphere	0.25 M Na ₂ SO ₄	200	1	[66]
MnO ₂ nanosheet	0.1 M Na ₂ SO ₄	182	0.1	[67]
MnO ₂ microsphere	1 M Na ₂ SO ₄	190	0.5	[68]
MnO ₂ nanosheet array	1 M Na ₂ SO ₄	201	1	[69]
MnO ₂ tubular nanostructure	1 M Na ₂ SO ₄	315	0.2	[70]
Mesoporous MnO ₂ particle	1 M Na ₂ SO ₄	173	0.25	[71]
Porous nano-MnO ₂	1 M Na ₂ SO ₄	198	0.28	[72]
Electrodeposited MnO ₂ -nanopillars	1 M Na ₂ SO ₄	603	10.0	[73]

Symmetric pseudocapacitor with nickel foam substrate

Further investigation of the OLC and OLC/MnO₂ as a full cell symmetric supercapacitor were carried out using nickel foam as the current collector considering its lower cost and better performance at half-cell experiments compared to platinum. **Fig. 7** shows CVs

(Fig. 7a,c) and galvanostatic charge-discharge curves (Fig. 7b,d) of the OLC and OLC/MnO₂ nanohybrid. In agreement with three-electrode experiment, two-electrode data of OLC/MnO₂ nanohybrid shows much higher gravimetric capacitance compared to OLC electrodes. The OLC/MnO₂ is capable of cycling at very high current densities (up to 10 A g⁻¹, Fig. 7d), yielding a high specific capacitance as suitable for high power energy storage applications.

Table 3 summarizes the values of the capacitance parameters obtained in comparison with literature, and it is evident that OLC/MnO₂ nanohybrid exhibits higher performance (in terms of power density or rate capability) than many state-of-the-art MnO₂-based pseudocapacitors. Note that there is no known report on symmetric supercapacitor based on birnessite-type MnO₂ in the literature so far; yet, the latter is of utmost importance to transition to actual devices and not just laboratory-relevant data.

Table 3: Comparison of electrochemical performance of some MnO₂-based aqueous symmetric electrochemical capacitors.

Electrode	Electrolyte	V_{\max} (V)	C_{sp} (F g ⁻¹)	E_{sp} (Wh kg ⁻¹)	P_{\max} (kW kg ⁻¹)	[#] EDR (Ω cm ²)	Reference
OLC	1 M Na ₂ SO ₄	0.8	12	0.3	2.9	7.8	This work
OLC/MnO ₂	1 M Na ₂ SO ₄	0.8	254	5.6	74.8	3.1	This work
GF/MnO ₂	1 M Na ₂ SO ₄	1.0	240	8.3	20.0	~11.9	[74]
C/MnO ₂ DNTAs	1 M Na ₂ SO ₄	0.8	161	35.0	16.0	~20	[75]
CNOs/MnO ₂	0.5 M H ₂ SO ₄	1.0	575	30.1	17.9	~7	[30]
GN-(γ-MnO ₂ /CNT)	6 M KOH	1.0	310	43.0	26.0	~3.2	[76]
MnO ₂ /PDDA/CNO	1 M Na ₂ SO ₄	0.9	218.6	6.14	-	~8.3	[77]

Key: GN = graphene nanosheets; GF = graphene foam; CNT = carbon nanotubes; DNTA = double-walled nanotube arrays (DNTAs); CNOs = carbon nano-onions; PDDA: polydiallyldimethylammonium chloride. [#]The EDR (equivalent distributed resistance) values were obtained prior to stability studies, and were converted to the Ω cm² based on the information we extracted from the cited reports.

Voltage-holding (or floating) experiments represent a reliable analysis method for establishing long-term stability of supercapacitor electrodes.^{60,61} In this work, the OLC/MnO₂ nanohybrid exhibited excellent stability during voltage-holding over 50 h at 1 A g⁻¹ (see *Supporting Information*, **Fig. S4**). This performance has been illustrated by the gradual decrease in the specific capacitance as the current is kept constant at high potential, retaining *ca.* 200 F g⁻¹ (i.e., approximately 90% of its initial capacitance of 220 F g⁻¹). The excellent stability of the OLC/MnO₂ nanohybrid showed that this device can be charged and discharged without significant deterioration in efficiency. These values correspond with a maximum specific energy of 5.6 Wh kg⁻¹ and an excellent power density of 74.8 kW kg⁻¹. The improved performance of this hybrid symmetric pseudocapacitor is attributed to the combination of the high electrical conductivity of OLC with the highly reversible redox reactions (pseudocapacitance) arising from the nanostructured MnO₂ material.

EIS data were acquired prior and post-floating experiments for the OLC/MnO₂ nanohybrid material (**Fig. 8**, and *Supporting Information Fig. S5*) and OLC alone (see *Supporting Information*, **Fig. S6**). The equivalent distributed resistance (EDR), comprising both the equivalent series resistance (ESR) and the ionic resistance within the porous structure (i.e., RC semicircle), was obtained by extrapolating the vertical portion of the plot to the real axis. The OLC/MnO₂ device shows a lower EDR (3.1 Ω cm²) compared to the OLC alone (7.8 Ω cm²). However, the RC semicircle for the OLC/MnO₂ is slightly bigger (~ 1.8 Ω cm²) than that of the OLC alone (~ 1.2 Ω cm²), meaning that ionic resistance within the porous structure of the pure EDLC (OLC alone) is increased for the OLC/MnO₂ pseudocapacitor. From the Bode plots, the phase angle for the pure OLC is -85° (which is close to the -90° for an ideal EDLC) compared to the OLC/MnO₂ which is -80°, further indicating the pseudocapacitive behavior of the OLC/MnO₂ device. The knee frequency (f_0 , ϕ

= -45°) describes the maximum frequency at which the capacitive behavior is dominant, and is a measure of the power capability of a supercapacitor; the higher the f_0 the more rapidly the supercapacitor can be charged and discharged or the higher the power density that can be achieved from the supercapacitor. The values of the f_0 was *ca.* 25 Hz for the OLC/MnO₂ (time constant \sim 40 ms) and 5 Hz (time constant \sim 0.2 s) for the OLC, further corroborates the higher-power performance of the OLC/MnO₂ over its OLC counterpart. It is important to note that the f_0 values remain approximately the same for both devices before and after 50 h voltage holding. This result shows that most of the stored energy in OLC/MnO₂ is accessible up to 25 Hz, that is, energy output available on millisecond time scale. It should be stated here that most commercially available supercapacitors, including those designed for higher power applications, operate at frequencies less than 1 Hz.⁶²

Conclusions

This work investigated the electrochemical performance of highly graphitized onion-like carbon integrated with nanostructured birnessite-type MnO₂ materials (OLC/MnO₂) when used as a symmetrical pseudocapacitor device. From the half-cell experiment, the OLC/MnO₂ nanohybrid exhibited better performance when using Ni foam as the current collector (in terms of specific capacitance and rate capability) compared to a Pt disc substrate. Based on its excellent performance, Ni foam was used to fabricate the OLC/MnO₂ symmetric pseudocapacitor. The device gave excellent electrochemical performance with a specific capacity of 408 F g⁻¹, specific energy density of 5.6 Wh kg⁻¹, power density of 74.8 kW kg⁻¹, capacity retention upon long-hour voltage-holding and cycling, very low equivalent distributed resistance (EDR \approx 3 Ω cm²), and very short RC time constant (40 ms). Using such a nanohybrid material, it is possible to overcome the main limitation of MnO₂, namely its poor electrical conductivity (10^{-6} – 10^{-5} S cm⁻¹) and to exploit its main advantages, namely low-cost, high abundance, and environmentally-friendliness, for high power energy storage

devices. Indeed, the electrochemical properties of OLC/MnO₂ nanohybrid as high-rate energy storage device have great potential for the development of high power aqueous-based supercapacitors that can be deployed for high-power technological applications.

Acknowledgements

This work was funded by the CSIR as well as the South Africa's Department of Science and Technology (DST) and National Research Foundation (NRF) under the "*Nanotechnology Flagship Programme*" (supercapacitors and fuel cell project, Grant No: 69849). KM thanks the DST/NRF for scarce skill doctoral scholarship. PME and KR thank the NRF for postdoctoral fellowships. CSIR, INM, and Saarland University are partners in the CREATE-Network funded by the European Commission. The INM is part of the Leibniz Research Alliance Energy Transition (LVE). The authors acknowledge funding from the German Federal Ministry for Research and Education (BMBF) in support of the nanoEES^{3D} project (award number 03EK3013) as part of the strategic funding initiative energy storage framework. MZ and VP thank Prof. Eduard Arzt (INM) for his continuing support. Dipl.-Ing. Sebastian Slawik and Prof. Frank Mücklich (Chair of Functional Materials, Saarland University) are thanked for their support regarding X-ray diffraction.

References

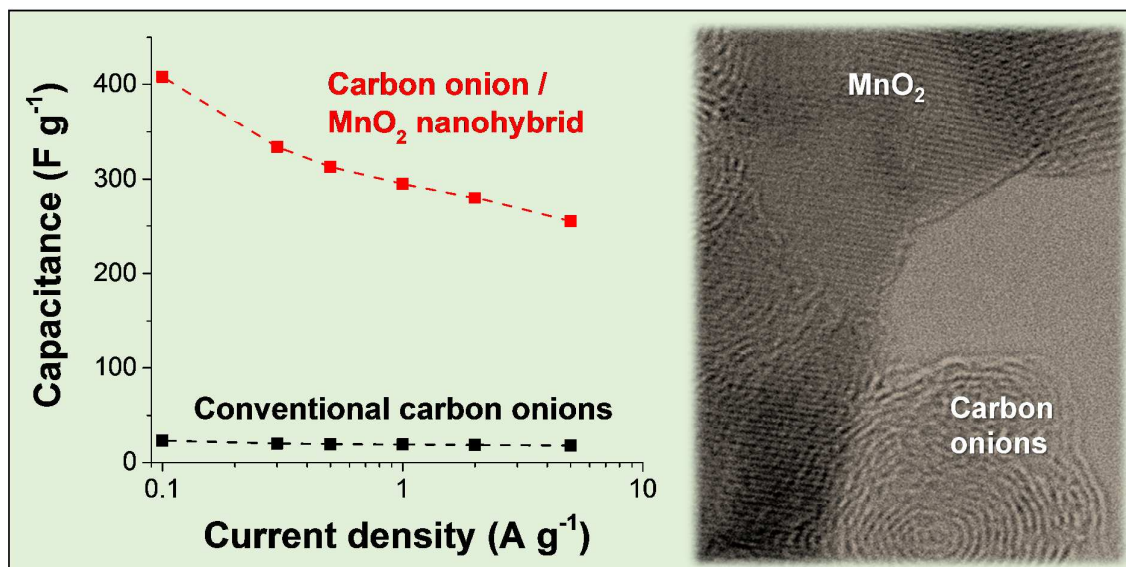
- [1] F. Béguin, V. Presser, a Balducci, E. Frackowiak, *Adv. Mater.* (2014) 2219.
- [2] A. Burke, *J. Power Sources* 91 (2000) 37.
- [3] P. Simon, Y. Gogotsi, B. Dunn, *Science* 343 (2014) 1210.
- [4] V. Augustyn, P. Simon, B. Dunn, *Energy Environ. Sci.* (2014).
- [5] P. Simon, Y. Gogotsi, *Nat. Mater.* 7 (2008) 845.
- [6] Y. Zhai, Y. Dou, D. Zhao, P.F. Fulvio, R.T. Mayes, S. Dai, *Adv. Mater.* 23 (2011) 4828.
- [7] B.E. Conway, V. Birss, J. Wojtowicz, *J. Power Sources* 66 (1997) 1.
- [8] R. Kotz, M. Carlen, *Electrochim. Acta* 45 (2000) 2483.
- [9] E. Frackowiak, F. Béguin, *Carbon N. Y.* 39 (2001) 937.
- [10] J.R. Miller, *Science* 335 (2012) 1312.
- [11] C. Largeot, C. Portet, J. Chmiola, P. Taberna, Y. Gogotsi, P. Simon, (2008) 2730.
- [12] E. Frackowiak, *Phys. Chem. Chem. Phys.* 9 (2007) 1774.
- [13] A.T. Chidembo, K.I. Ozoemena, B.O. Agboola, V. Gupta, G.G. Wildgoose, R.G. Compton, *Energy Environ. Sci.* 3 (2010) 228.
- [14] A. Bello, K. Makgopa, M. Fabiane, D. Dodoo-Ahrin, K.I. Ozoemena, N. Manyala, *J. Mater. Sci.* 48 (2013) 6707.
- [15] C.J. Jafta, F. Nkosi, L. le Roux, M.K. Mathe, M. Kebede, K. Makgopa, Y. Song, D. Tong, M. Oyama, N. Manyala, S. Chen, K.I. Ozoemena, *Electrochim. Acta* (2013) 2.
- [16] E.J. Ra, E. Raymundo-Piñero, Y.H. Lee, F. Béguin, *Carbon N. Y.* 47 (2009) 2984.
- [17] J. Li, E. Liu, W. Li, X. Meng, S. Tan, *J. Alloys Compd.* 478 (2009) 371.
- [18] U. Fischer, R. Saliger, V. Bock, *J. Porous Mater.* 285 (1997) 281.
- [19] Y. Wang, Z.J. Han, S.F. Yu, R.R. Song, H.H. Song, K. (Ken) Ostrikov, H.Y. Yang, *Carbon N. Y.* 64 (2013) 230.
- [20] Y. Wang, F. Yan, S.W. Liu, A.Y.S. Tan, H. Song, X.W. Sun, H.Y. Yang, *J. Mater. Chem. A* 1 (2013) 5212.

- [21] D.M. Anjos, J.K. McDonough, E. Perre, G.M. Brown, S.H. Overbury, Y. Gogotsi, V. Presser, *Nano Energy* (2013).
- [22] I. Kovalenko, D.G. Bucknall, G. Yushin, *Adv. Funct. Mater.* 20 (2010) 3979.
- [23] Y. Gao, Y.S. Zhou, M. Qian, X.N. He, J. Redepenning, P. Goodman, H.M. Li, L. Jiang, Y.F. Lu, *Carbon N. Y.* 51 (2013) 52.
- [24] E.G. Bushueva, P.S. Galkin, a. V. Okotrub, L.G. Bulusheva, N.N. Gavrilov, V.L. Kuznetsov, S.I. Moiseev, *Phys. Status Solidi* 245 (2008) 2296.
- [25] C. Portet, G. Yushin, Y. Gogotsi, *Carbon N. Y.* 45 (2007) 2511.
- [26] J.K. McDonough, A.I. Frolov, V. Presser, J. Niu, C.H. Miller, T. Ubieto, M. V. Fedorov, Y. Gogotsi, *Carbon N. Y.* 50 (2012) 3298.
- [27] I. Suarez-Martinez, N. Grobert, C.P. Ewels, *Carbon N. Y.* 50 (2012) 741.
- [28] V.N. Mochalin, O. Shenderova, D. Ho, Y. Gogotsi, *Nat. Nanotechnol.* 7 (2012) 11.
- [29] D. Pech, M. Brunet, H. Durou, P. Huang, V. Mochalin, Y. Gogotsi, P.-L. Taberna, P. Simon, *Nat. Nanotechnol.* 5 (2010) 651.
- [30] M.V.K. Azhagan, M. V. Vaishampayan, M. V. Shelke, *J. Mater. Chem. A* 2 (2014) 2152.
- [31] V.L. Kuznetsov, A.L. Chuvilin, Y. V. Butenko, I.Y. Mal'kov, V.M. Titov, *Chem. Phys. Lett.* 222 (1994) 343.
- [32] Daniel Urgate, *Nature* 359 (1992) 707.
- [33] S. Iijima, *J. Crystal Growth* 50 (1980) 675.
- [34] M. Choucair, J.A. Stride, *Carbon N. Y.* 50 (2012) 1109.
- [35] C. Julien, *Solid State Ionics* 159 (2003) 345.
- [36] C. Matei Ghimbeu, A. Malak-Polaczyk, E. Frackowiak, C. Vix-Guterl, *J. Appl. Electrochem.* 44 (2013) 123.
- [37] P. Yu, X. Zhang, Y. Chen, Y. Ma, *Mater. Lett.* 64 (2010) 1480.
- [38] B. Ming, J. Li, F. Kang, G. Pang, Y. Zhang, L. Chen, J. Xu, X. Wang, *J. Power Sources* 198 (2012) 428.
- [39] M. Huang, Y. Zhang, F. Li, L. Zhang, R.S. Ruoff, Z. Wen, Q. Liu, *Sci. Rep.* 4 (2014) 3878.
- [40] X. Zhang, X. Sun, H. Zhang, D. Zhang, Y. Ma, *Mater. Chem. Phys.* 137 (2012) 290.

- [41] X. Zhang, P. Yu, H. Zhang, D. Zhang, X. Sun, Y. Ma, *Electrochim. Acta* 89 (2013) 523.
- [42] Y. Wang, S.F. Yu, C.Y. Sun, T.J. Zhu, H.Y. Yang, *J. Mater. Chem.* 22 (2012) 17584.
- [43] P. Yang, Y. Ding, Z. Lin, Z. Chen, Y. Li, P. Qiang, M. Ebrahimi, W. Mai, C.P. Wong, Z.L. Wang, *Nano Lett.* 14 (2014) 731.
- [44] Z.-S. Wu, W. Ren, D.-W. Wang, F. Li, B. Liu, H.-M. Cheng, *ACS Nano* 4 (2010) 5835.
- [45] H. Xia, Y. Wang, J. Lin, L. Lu, *Nanoscale Res. Lett.* 7 (2012) 33.
- [46] H. Yang, J. Jiang, W. Zhou, L. Lai, L. Xi, Y.M. Lam, Z. Shen, B. Khezri, T. Yu, *Nanoscale Res. Lett.* 6 (2011) 531.
- [47] D. Weingarh, M. Zeiger, N. Jäckel, M. Aslan, G. Feng, V. Presser, *Adv. Energy Mater.* (2014) In Press.
- [48] S. Brunauer, P.H. Emmett, E. Teller, *J. Am. Chem. Soc.* 60 (1938) 309.
- [49] G.Y. Gor, M. Thommes, K. a. Cychosz, A. V. Neimark, *Carbon N. Y.* 50 (2012) 1583.
- [50] Y. V. Butenko, V.L. Kuznetsov, a. L. Chuvilin, V.N. Kolomiichuk, S. V. Stankus, R. a. Khairulin, B. Segall, *J. Appl. Phys.* 88 (2000) 4380.
- [51] T.K. Gupta, B.P. Singh, V.N. Singh, S. Teotia, A.P. Singh, I. Elizabeth, S.R. Dhakate, S.K. Dhawan, R.B. Mathur, *J. Mater. Chem. A* 2 (2014) 4256.
- [52] K. Bogdanov, A. Fedorov, V. Osipov, T. Enoki, K. Takai, T. Hayashi, V. Ermakov, S. Moshkalev, A. Baranov, *Carbon N. Y.* 73 (2014) 78.
- [53] D. Yang, M. Wang, *Chem. Mater.* 13 (2001) 2589.
- [54] F.-J. Liu, *J. Power Sources* 182 (2008) 383.
- [55] Z. Li, Y. Mi, X. Liu, S. Liu, S. Yang, J. Wang, *J. Mater. Chem.* 21 (2011) 14706.
- [56] Y.-K. Hsu, Y.-C. Chen, Y.-G. Lin, L.-C. Chen, K.-H. Chen, *J. Mater. Chem.* 22 (2012) 2733.
- [57] M.C. Biesinger, B.P. Payne, A.P. Grosvenor, L.W.M. Lau, A.R. Gerson, R.S.C. Smart, *Appl. Surf. Sci.* 257 (2011) 2717.
- [58] T.E. Rufford, D. Hulicova-Jurcakova, K. Khosla, Z. Zhu, G.Q. Lu, *J. Power Sources* 195 (2010) 912.
- [59] L.-Y. Lin, M.-H. Yeh, J.-T. Tsai, Y.-H. Huang, C.-L. Sun, K.-C. Ho, *J. Mater. Chem. A* 1 (2013) 11237.

- [60] D. Weingarth, a. Foelske-Schmitz, R. Kötzt, J. Power Sources 225 (2013) 84.
- [61] P. Ratajczak, K. Jurewicz, F. Béguin, J. Appl. Electrochem. 44 (2013) 475.
- [62] J.R. Miller, Electrochem. Soc. Proc. Ser. PV95-29 (1996) 246.
- [63] Y. Zhao, P. Jiang, S.-S. Xie, J. Power Sources 239 (2013) 393.
- [64] W. Li, Q. Liu, Y. Sun, J. Sun, R. Zou, G. Li, X. Hu, G. Song, G. Ma, J. Yang, Z. Chen, J. Hu, J. Mater. Chem. 22 (2012) 14864.
- [65] Y. Zhang, G. Li, Y. Lv, L. Wang, A. Zhang, Y. Song, B. Huang, Int. J. Hydrogen Energy 36 (2011) 11760.
- [66] Y. Zhang, C. Sun, P. Lu, K. Li, S. Song, D. Xue, CrystEngComm 14 (2012) 5892.
- [67] H. Jang, S. Suzuki, M. Miyayama, J. Electrochem. Soc. 159 (2012) A1425.
- [68] W. Ko, L. Chen, Y. Chen, W. Chen, K. Lu, J. Yang, Y. Yen, K. Lin, (2013).
- [69] M. Kundu, L. Liu, J. Power Sources 243 (2013) 676.
- [70] J. Zhu, W. Shi, N. Xiao, X. Rui, H. Tan, X. Lu, H.H. Hng, J. Ma, Q. Yan, ACS Appl. Mater. Interfaces 4 (2012) 2769.
- [71] L. Chen, N. Gu, R. Ding, L. Qi, H. Wang, J. Solid State Electrochem. 17 (2013) 2579.
- [72] H.-Q. Wang, G. Yang, Q.-Y. Li, X.-X. Zhong, F.-P. Wang, Z.-S. Li, Y. Li, New J. Chem. 35 (2011) 469.
- [73] Z. Yu, B. Duong, D. Abbitt, J. Thomas, Adv. Mater. 25 (2013) 3302.
- [74] A. Bello, O.O. Fashedemi, J.N. Lekitima, M. Fabiane, D. Dodoo-Arhin, K.I. Ozoemena, Y. Gogotsi, A.T. Charlie Johnson, N. Manyala, AIP Adv. 3 (2013) 082118.
- [75] Q. Li, X.-F. Lu, H. Xu, Y.-X. Tong, G.-R. Li, ACS Appl. Mater. Interfaces 6 (2014) 2726.
- [76] R.B. Rakhi, W. Chen, D. Cha, H.N. Alshareef, Adv. Energy Mater. 2 (2012) 381.
- [77] R. Borgohain, J.P. Selegue, Y.-T. Cheng, J. Mater. Chem. A. 2 (2014) 20367

Graphic Abstract



Carbon onion/birnessite-type manganese oxide nanohybrid symmetric pseudocapacitor exhibits excellent capacitive properties compared to the conventional carbon onion symmetric supercapacitor.

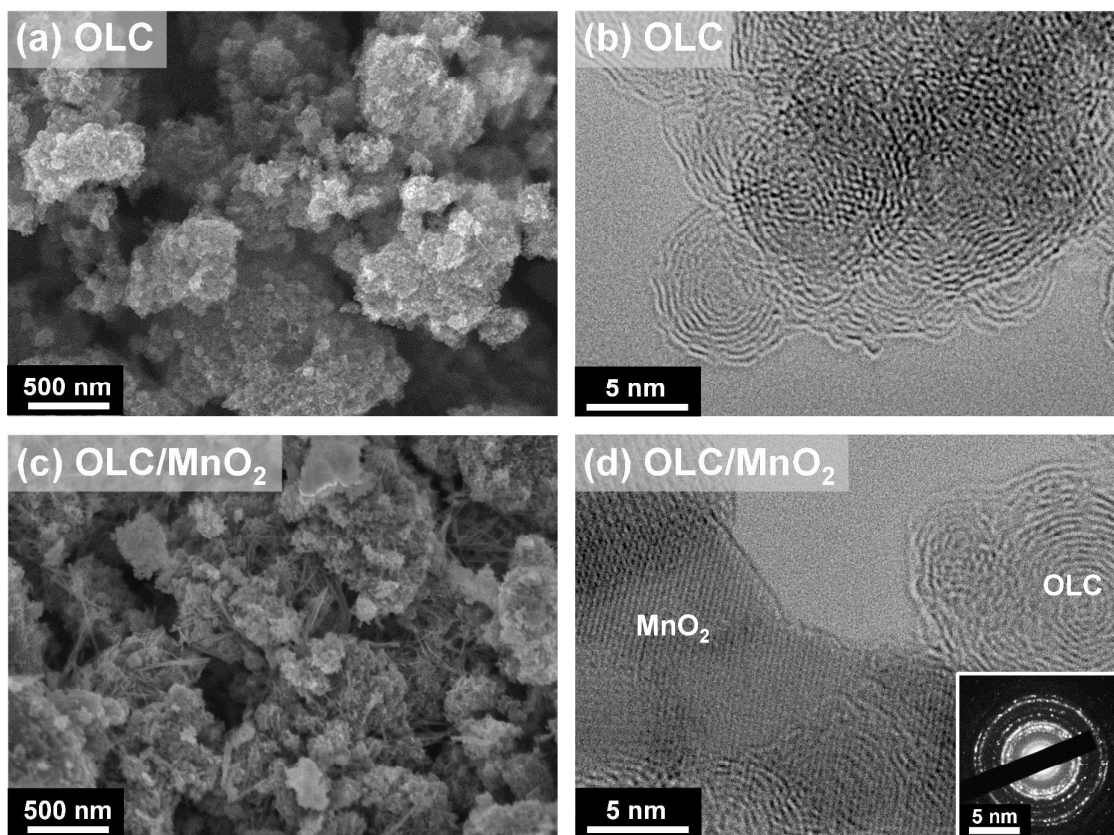


Fig. 1. SEM images of (a) OLC, and (c) OLC/MnO₂ nanohybrid, TEM images of (b) OLC and (d) OLC/MnO₂ nanohybrid. Inset is the corresponding SAED pattern of (d).

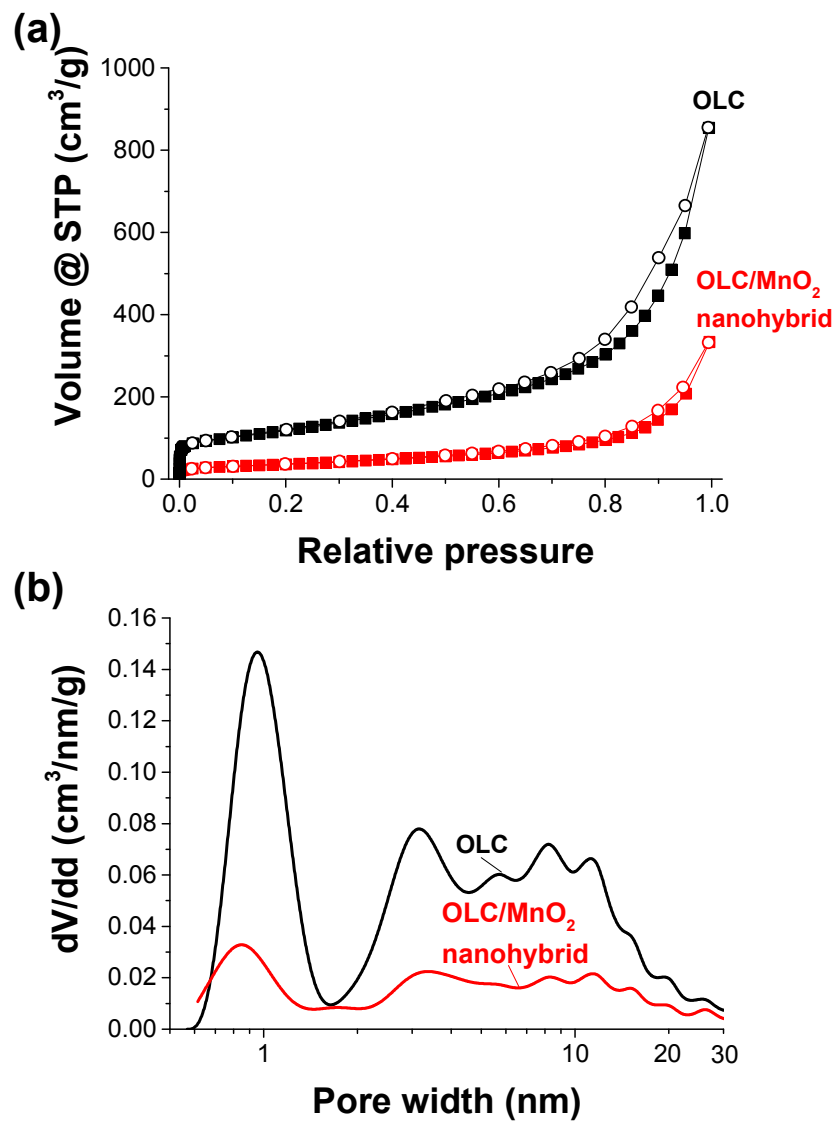


Fig. 2: (a) Pore size distribution and (b) nitrogen adsorption-desorption isotherms at -196 °C, overlays of OLC and OLC/MnO₂ nanohybrid.

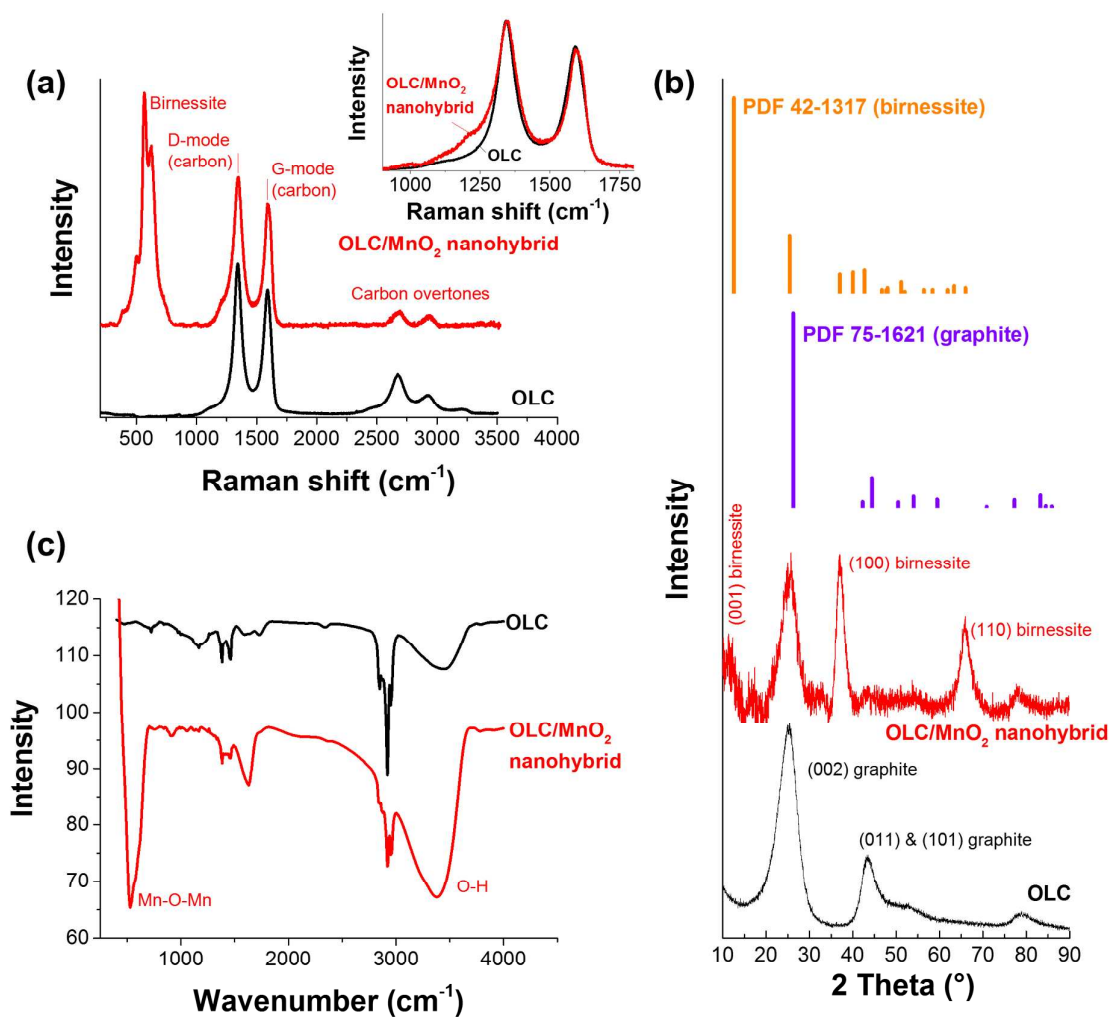


Fig. 3: (a) Raman spectra, (b) X-ray diffraction pattern, and (c) FTIR spectra of OLC and OLC/MnO₂ nanohybrid.

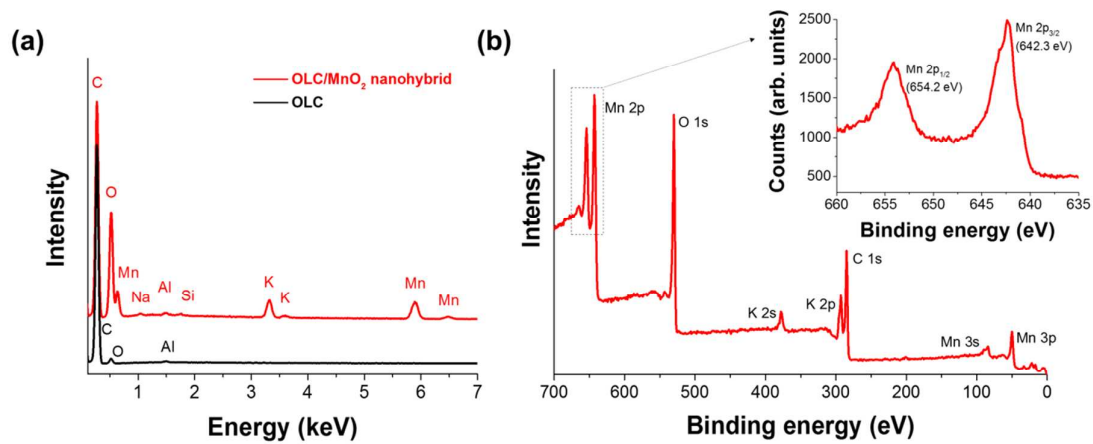


Fig. 4: (a) Energy dispersive X-ray (EDX) spectra of OLC and OLC/MnO₂ nanohybrid and (b) X-ray photoelectron spectrum (XPS) of the OLC/MnO₂ nanohybrid.

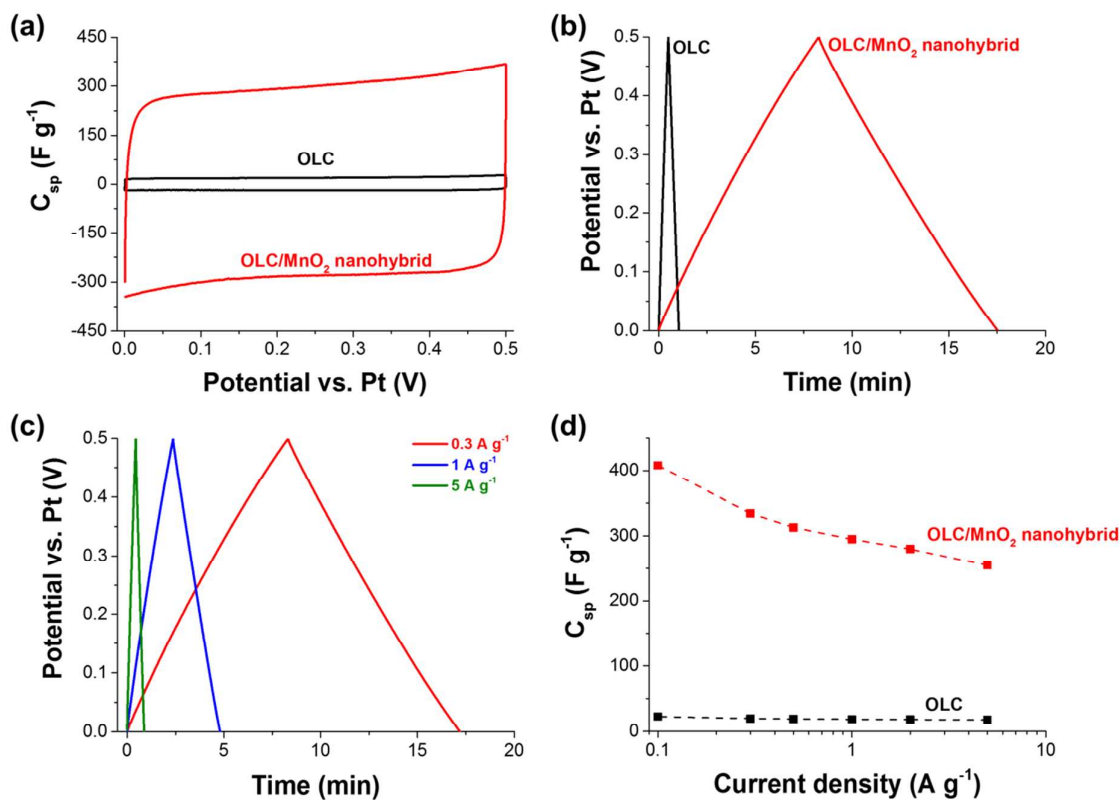


Fig. 5: 3-electrode configuration with a Pt disc as the current collector: (a) cyclic voltammograms at $2 mVs^{-1}$, (b) galvanostatic charge-discharge curves at $0.3 A g^{-1}$ comparing OLC and OLC/MnO₂ nanohybrid, (c) galvanostatic charge-discharge curves for OLC/MnO₂ nanohybrid at various current densities, and (d) C_{sp} vs current densities of OLC/MnO₂ nanohybrid. Electrolyte: aqueous 1M Na₂SO₄.

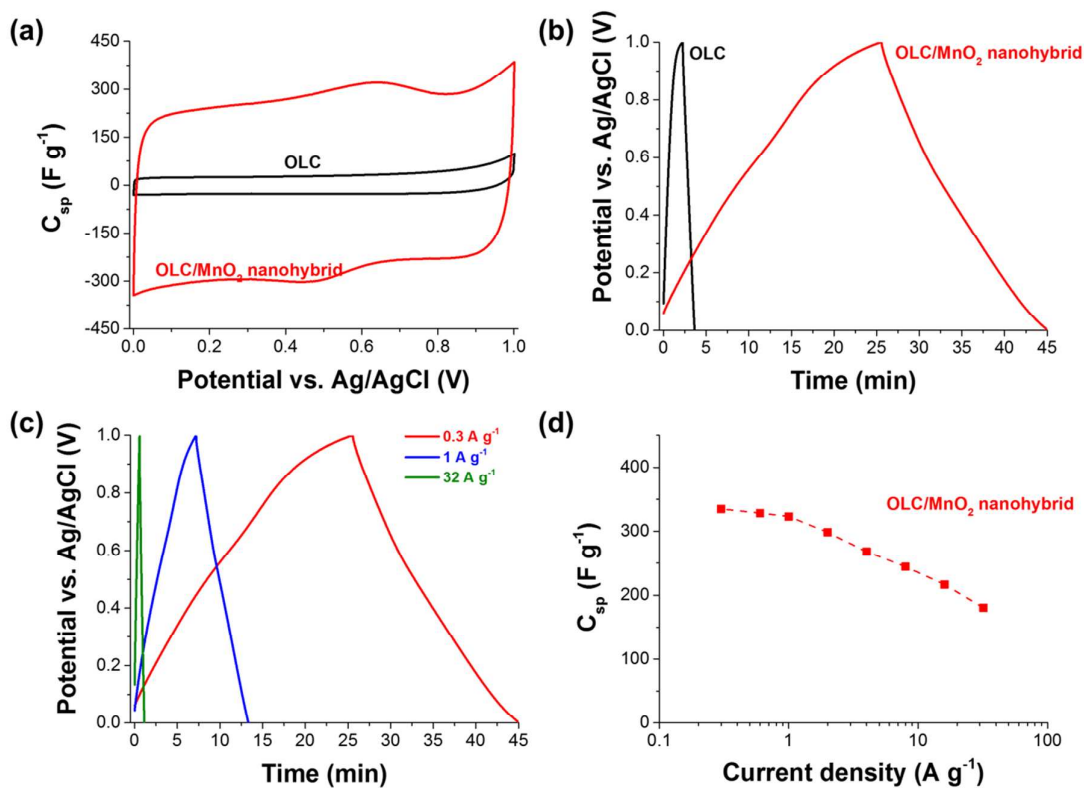


Fig. 6: 3-electrode configuration with Nickel foam as the current collector: (a) cyclic voltammograms at 5mVs^{-1} and (b) galvanostatic charge-discharge curves at $0.3\ A\ g^{-1}$ comparing OLC and OLC/MnO₂ nanohybrid, (c) galvanostatic charge-discharge curves for OLC/MnO₂ nanohybrid at various current densities, and (d) C_{sp} vs current densities of OLC/MnO₂ nanohybrid. Electrolyte: aqueous $1\text{M}\ Na_2SO_4$.

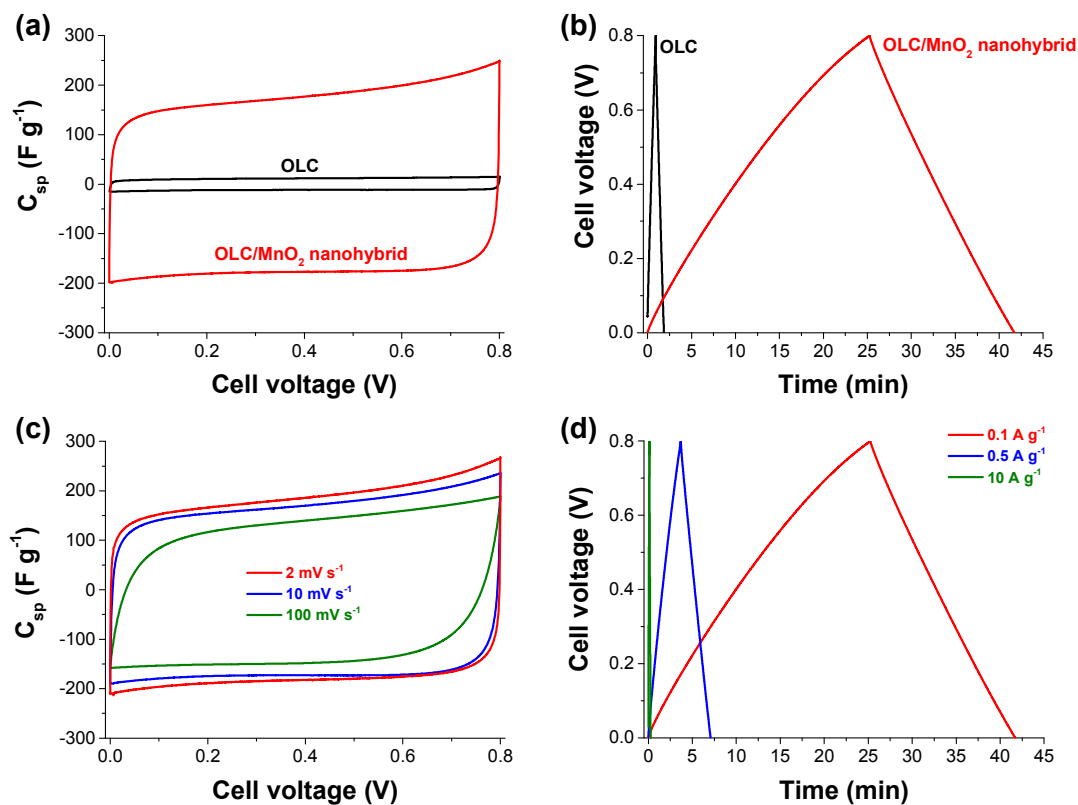


Fig. 7: Nickel foam based 2-electrode (symmetric) configuration: (a) comparative cyclic voltammograms for OLC and OLC/MnO₂ at 5 mV/s, (b) comparative galvanostatic charge-discharge curves for OLC and OLC/MnO₂ at 0.1 A g⁻¹, and, (c) CVs at different scan rates for OLC/MnO₂ (d) comparative galvanostatic charge-discharge curves for OLC and OLC/MnO₂ nanohybrid at different current densities. Electrolyte: aqueous 1M Na₂SO₄.

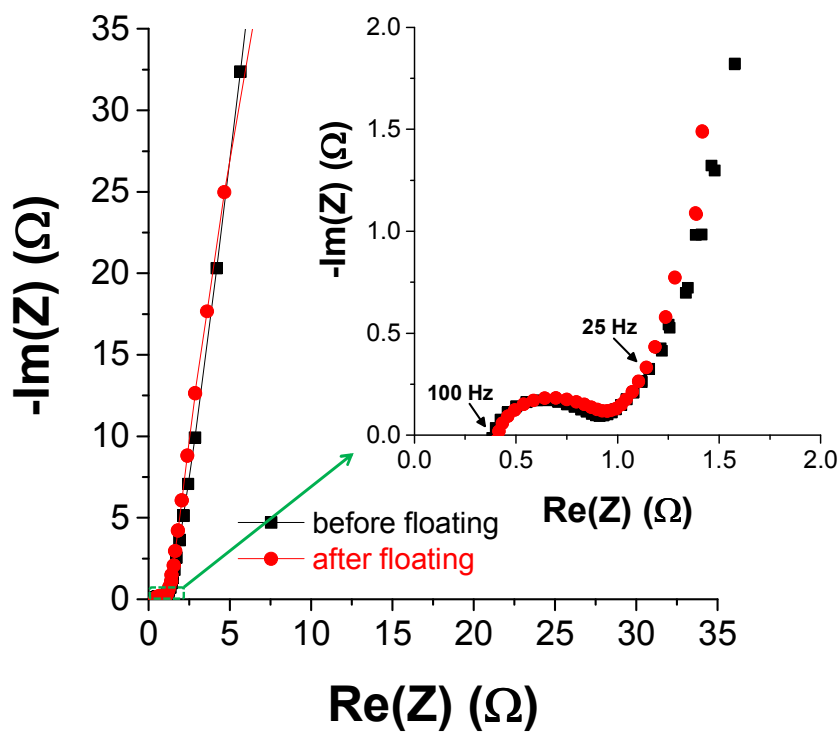


Fig. 8: Nyquist plot for the OLC/MnO₂ symmetric pseudocapacitor before and after 50 h voltage holding experiments. The inset is the expanded portion of the high frequency region. Electrolyte: aqueous 1M Na₂SO₄.

GRAPHICAL ABSTRACT

High-rate aqueous symmetric pseudocapacitor based on highly graphitized onion-like carbon/birnessite-type manganese oxide nanohybrids

Katlego Makgopa,¹ Paul M. Ejikeme,¹ Charl J. Jafta,² Kumar Raju,²
Marco Zeiger,^{3,4} Volker Presser,^{3,4*} and Kenneth I. Ozoemena^{1,2*}

¹ Department of Chemistry, University of Pretoria, Pretoria 0002, South Africa

² Energy Materials, Materials Science and Manufacturing, Council for Scientific & Industrial Research (CSIR), Pretoria 0001, South Africa

³ INM - Leibniz Institute for New Materials, 66123 Saarbrücken, Germany

⁴ Saarland University, 66123 Saarbrücken, Germany

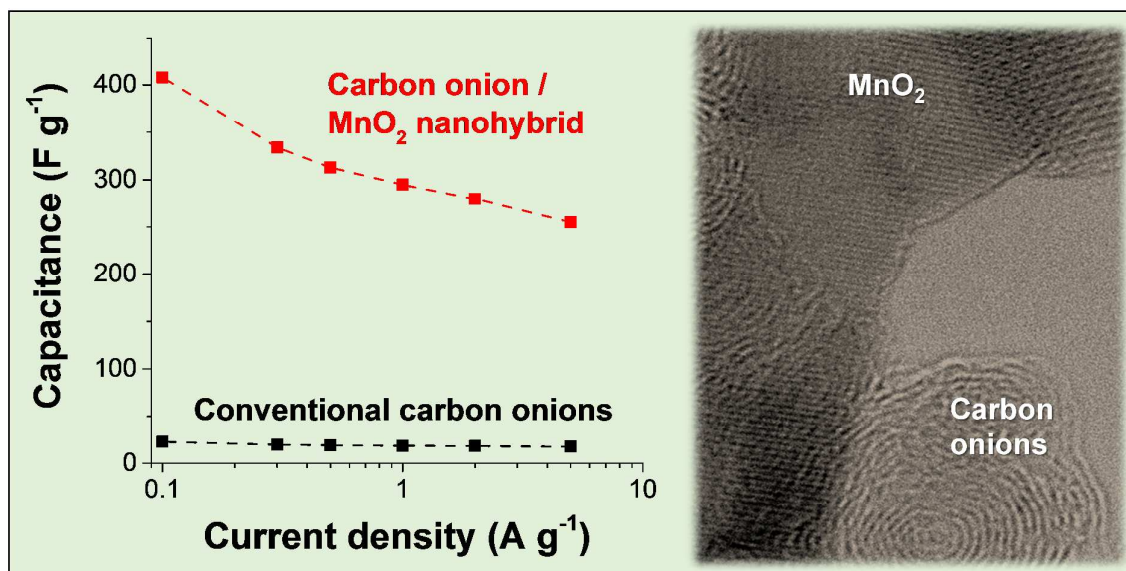
Revised manuscript for *J. Mater. Chem. A* (Manuscript ID: TA-ART-10-2014-005697)

*Authors to whom correspondence should be addressed:

(K.I. Ozoemena): Tel.: +27128413664; Fax: +27128412135; E-mail: kozoemena@csir.co.za;

(V. Presser): Tel.: +496819300177; Fax: +496819300223; E-mail: volker.presser@inm-gmbh.de

Graphic Abstract



Carbon onion/birnessite-type manganese oxide nanohybrid symmetric pseudocapacitor exhibits excellent capacitive properties compared to the conventional carbon onion symmetric supercapacitor.